IAEA
International Atomic Energy Agency

20th IAEA Fusion Energy Conference
Vilamoura, Portugal, 1-6 November 2004

IAEA-CN-116/TH/1-6

Profile Formation and Sustainment of Autonomous Tokamak Plasma with Current Hole Configuration

N. Hayashi, T. Takizuka and T. Ozeki

Japan Atomic Energy Research Institute,
Naka Fusion Research Establishment,
801-1 Naka, Ibaraki, 311-0193 JAPAN

Profile Formation and Sustainment of Autonomous Tokamak Plasma with Current Hole Configuration

N. Hayashi, T. Takizuka, T. Ozeki

Japan Atomic Energy Research Institute, Naka, Ibaraki, 311-0193 Japan
e-mail contact of main author: hayashin@fusion.naka.jaeri.go.jp

Abstract. We have investigated the profile formation and sustainment of tokamak plasmas with the current hole (CH) configuration by using 1.5D time-dependent transport simulations. A model of the current limit inside the CH on the basis of the Axisymmetric Tri-Magnetic-Islands equilibrium is introduced into the transport simulation. We found that a transport model with the sharp reduction of anomalous transport in the reversed-shear (RS) region can reproduce the time evolution of profiles observed in JT-60U experiments. The transport becomes neoclassical-level in the RS region, which results in the formation of profiles with internal transport barrier (ITB) and CH. The CH plasma has an autonomous property because of the strong interaction between a pressure profile and a current profile through the large bootstrap current fraction. The ITB width determined by the neoclassical-level transport agrees well with that measured in JT-60U. The energy confinement inside the ITB agrees with the scaling based on the JT-60U data. The scaling means the autonomous limitation of energy confinement in the CH plasma. The plasma with the large CH is sustained with the full current drive by the bootstrap current. The plasma with the small CH and the small bootstrap current fraction shrinks due to the penetration of inductive current. This shrink is prevented and the CH size can be controlled by the appropriate external current drive (CD). The CH plasma is found to respond autonomically to the external CD.

1. Introduction

The current hole (CH) with nearly zero current in the central region has been observed in several tokamaks[1,2]. Increase of the off-central noninductive current is the key for the CH formation. Lower hybrid current drive (LHCD) was applied to form the CH in JET. In JT-60U, the bootstrap current induced by the strong internal transport barrier (ITB) plays a dominant role to form the CH. In a CH plasma, high confinement performance is achieved due to the formation of strong ITB in the reversed-shear (RS) region. The CH plasma has an autonomous property because of the interaction between a pressure profile and a current profile through the large bootstrap current. The CH plasma is considered an attractive candidate for the economic steady-state reactor due to its high confinement and high bootstrap current fraction. It is necessary to clarify the physical mechanism of profile formation and sustainment of the autonomous CH plasma.

Several theoretical studies have been done to explain the physical mechanism of CH. An idea of a new equilibrium of a strongly-RS plasma with a CH was proposed[3] instead of the MHD-instability based ideas[4-6]. The equilibrium called "Axisymmetric Tri-Magnetic-Islands (ATMI) equilibrium" has three islands along the R direction (a central-negative-current island and two side-positive-current islands) and two x-points along the Z direction. The ATMI equilibrium is stable with the elongation coils when the current in the ATMI region is limited to be small. The existence of the ATMI equilibrium has been numerically confirmed by solving Grad-Shafranov equation[7].

The 1.5 dimensional (1.5D) transport code is one of the effective methods to simulate the profile formation and sustainment of the CH plasma. For example, the CH formation by LHCD in JET was successfully simulated by solving the current diffusion equation[8]. The impact on different heating and current drive methods on the early q-profile evolution in JET RS plasmas was investigated by the JETTO transport code[9]. These studies focused mainly the formation of CH or RS plasmas induced by the external CD. In general, the formation of

negative currents in the central region prevents the 1.5D transport simulation from going on. A model of the current limit inside CH is effective to run the simulation. Additionally, an appropriate transport model is required to simulate the strong ITB observed in CH plasmas.

In this paper, we investigate the profile formation and sustainment of the autonomous CH plasma by 1.5D time-dependent transport simulations for JT-60U parameters. In the next section, we explain a current limit model based on the ATMI equilibrium and a transport model based on both theories and experiments. The simulation model is validated by comparing with JT-60U experiments in Section 3. The physical mechanism of the formation of autonomous CH plasmas is shown. The ITB structure and the energy confinement are investigated and compared with JT-60U data in Sections 4 and 5. The sustainment and the control of autonomous CH plasmas by the external CD are examined in the last section.

2. Current Limit Model based on the ATMI Equilibrium and Transport Model

The 1.5D transport code self-consistently solves the 1D transport and current diffusion equations and the Grad-Shafranov equation of the MHD equilibrium in the 2D plane (R,Z). The transport equations are the continuity equation for the deuterium ion density, n_i, the power balance equations for the electron temperature, T_e, and the ion temperature, T_i, on the coordinate of the normalized minor radius, $\rho=(\Phi(\rho)/\Phi(1))^{0.5}$, defined by the square root of the toroidal flux Φ. Details of the transport code are shown in Ref.[10].

A model of the current limit inside the CH on the basis of the ATMI equilibrium is introduced into the 2D MHD equilibrium calculation. In the MHD equilibrium calculation, the current density in the CH region is assumed to be uniform. The value of the current inside CH remains to be small so that the stable condition of ATMI equilibrium is satisfied; $q_{ATMI}/q_a>\kappa_1^2 Z_c^2/a(Z_c-Z_x)$, where q_{ATMI}, q_a, κ_1, Z_c and Z_x denote the effective safety factor at the surface of the ATMI configuration, the engineering safety factor at the plasma surface, the ATMI effective ellipticity, the position of elongation coils and the x-points position, respectively[3]. The safety factor inside the CH region is assumed to be limited by a value of $q_{limit} = q_a \kappa_1^2 Z_c^2 /a(Z_c-Z_x)$ for the present model. As a result, the 1.5D transport simulation can continue. Note that, in the calculation of 1D current diffusion equation, the negative current exists inside the CH. A CH radius, ρ_{CH}, defined at the edge of the CH region, $q(\rho_{CH})=q_{limit}$, is self-determined and moves in the simulation.

We adopt a model of heat and particle diffusivities given as, $\chi_i=\chi_{neo}+\chi_{ano}$, $D_i=C_D D_{neo}+D_{ano}$, where χ_{neo} and D_{neo} denote the neoclassical ion thermal and particle diffusivities calculated by the matrix inversion method[11]. The value of C_D is constant in the range of $C_D\leq 1$ on the basis of JT-60U experimental analyses, i.e., the particle diffusivity was reduced below the ion neoclassical-level at ITB[12]. The electron heat diffusivity, χ_e, is assumed to be equal to χ_i for simplicity. The anomalous diffusivities, χ_{ano} and D_{ano}, are given as,

$$\chi_{ano} = D_{ano} = \chi_0 F(s-k\alpha), \qquad (1)$$

where χ_0 is a constant anomalous diffusivity. The negative magnetic shear is effective to stabilize the ballooning mode[13] and micro-instabilities[14]. The function F is sharply reduced for $s-k\alpha<0$ (Fig.1) where s, k and α denote the magnetic shear, an arbitrary constant and the normalized pressure gradient, respectively. This function with k=1 was originally developed for the ballooning type turbulence model[13]. The transport model

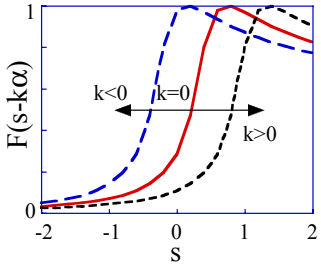

Fig.1 F versus s for various k values with α~1.

with k~0 seems to be reliable from the comparison with JT-60U experiments, where the ITB was located just inside the minimum q surface[1,15,16] and the heat diffusivities at the ITB region were reduced to the level of ion neoclassical diffusivity[12,15,17].

3. Comparison with JT-60U Experiment

In order to validate the simulation model, we compare the numerical results with a JT-60U shot[1] : R=3.2 m, a=0.8 m, κ=1.5, δ=0.12 and B_t=3.7 T. The time evolution of the plasma current, I_p, and the neutral-beam (NB) power, P_{NB}, is shown in Fig.2(a). For the JT-60U parameters of Z_c~2 m, Z_c–Z_x~0.6 m and q_a~4 at I_p=1.3 MA, the simulated safety factor inside the CH is limited by q_{limit}~30. An initial current profile is assumed to be weakly off-centered as shown in Fig.3(c), which is a similar one to the experiment. By giving an appropriate recycling coefficient of neutrals, the time evolution of averaged electron density almost agrees with the experiment ($<n_e> \approx 3\times10^{19}$ m^{-3} around t=3 s).

Figure 2(b) shows the time evolution of the normalized beta, $\beta_N=\beta_t$ a B_t / I_p [%·m·T/MA], and the poloidal beta, β_p, which agree well with the experiment. The time evolution of a ratio of B_p/B_t at different ρ positions also agrees with that measured by a motional Stark effect, as shown in Fig.2(c). A contour plot of parallel current density, j, is shown in Fig.2(d). The CH radius, ρ_{CH}, enlarges from t=0 s to 2 s. A peak value of the current density increases in accordance with the increase of bootstrap current density as shown in Fig.3(a). After the CH formation phase (t>2s), the CH radius and the radius at the peak of current density shrinks slowly as almost the same as in the experiment. Figure 2(e) and (f) show profiles of T_i, T_e, n_e, j and q at t=2 s, respectively. Each profile agrees well with the experimental one. The ITB is formed in the RS region. Inside the CH region, profiles of T_i, T_e and n_e are nearly flat. Simulation parameters are chosen as k=0, χ_0=2.6 m^2/s and C_D=1. Experimental observations in JT-60U are well reproduced by the present transport model with k~0. A radius at the ITB foot position, ρ_f, is almost the same as that at the minimum q surface, ρ_{qmin}. For the model with k~1 or −1, profiles and their time-evolution do not agree with the experiment. Sharp reduction of the transport to the neoclassical-level in the RS region (s≤0) realizes the

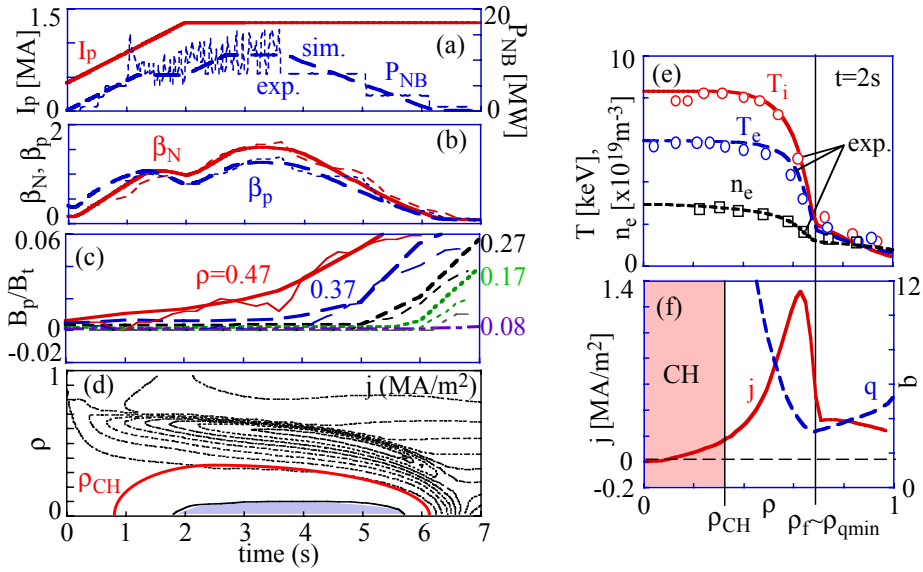

Fig.2 (a)-(b): Time evolution of (a) I_p, P_{NB}, (b) β_N, β_p, (c) B_p/B_t at various ρ position. In (a), thick line represents NB power modeled from experimental data of thin line. In (b)-(c), thick and thin lines represent simulation results and experimental data, respectively. (d): Contour plot of j (0.2 MA/m² division) where a broad line and shaded region denote CH radius ρ_{CH} and negative j, respectively. (e)-(f): Profiles of (e) T_i, T_e, n_e and (f) j, q at t=2 s where experimental data points are also shown.

autonomous formation of profiles with ITB and CH in RS plasmas, as observed in JT-60U experiments.

Physical mechanism of the CH formation and the growth of ITB structure are described here. Figure 3 shows the time evolution of profiles of (a) the bootstrap current density, j_{BS}, (b) the parallel electric field, $E=\eta(j-j_{BS})$, (c) j, (d) q, (e) χ_i, and (f) T_i on ρ during the current ramp-up (t=0-2 s with 0.4 s interval) for the simulation of Fig.2. The ITB is developed by the NB heating (see (f)) and the off-central bootstrap current increases in the RS region as shown in Fig.3(a). Therefore, the electric field decreases to negative value in the off-central region (see (b)). The dynamic behavior of E is easily seen in the simplified diffusion equation given as,

$$\frac{\partial \mathbf{E}}{\partial t} = \frac{\eta}{\mu_0}\nabla^2\mathbf{E} - \eta\frac{\partial \mathbf{j}_{BS}}{\partial t} \qquad (2)$$

The increase of j_{BS} results in the decrease of E through the second term in R.H.S of Eq.(2). The negative electric field diffuses into the central region through the first term in R.H.S as shown in Fig.3(b). The current in the central region drops due to the negative electric field and becomes negative around t=2 s as shown in Fig.3(c). The CH region is formed from t≈0.8 s. Outer current increases due to the bootstrap current. According to the evolution of j in Fig.3(c), the value of q increases in the central region, while q decreases in the outer region in Fig.3(d). In Fig.3(e), the transport is decreased to the neoclassical-level in the RS region, while the anomalous transport becomes dominant in the normal magnetic shear (NrS) region. The neoclassical transport is about one order smaller than the anomalous one in the NrS region. The diffusivity increases with q in the central region because of $\chi_{neo} \propto q^2$ as shown in Fig.3(e). On the other hand, in the outer region, the minimum value of χ_i is determined by χ_{neo} and decreases with q. As a result, as shown in Fig.3(f), an ITB is produced by the neoclassical-level transport in the RS region. Flat profile of T_i in the central region and the ITB shoulder are also due to the neoclassical-level transport with very high q. The CH formation progresses according to the following cycle. The ITB growth generates the large off-central bootstrap current and the CH is formed. The growth of off-central non-inductive current, i.e., the bootstrap current, is the key for the CH formation. A pressure profile and a current profile strongly interact with each other through the large bootstrap current fraction and a self-organized structure is formed. CH plasmas are strongly autonomous.

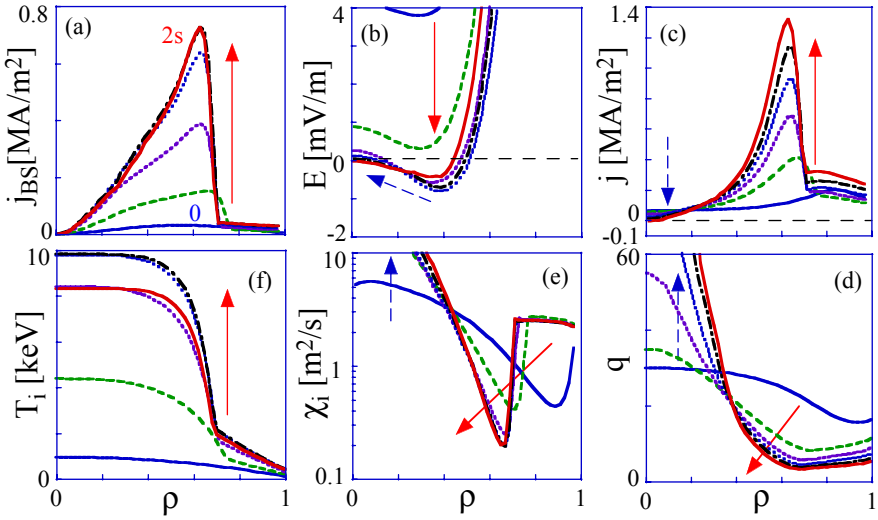

Fig.3 Time evolution of profiles of (a) j_{BS}, (b) E, (c) j, (d) q, (e) χ_i, and (f) T_i on ρ for simulation of Fig.2. In (b), electric field first decreases to negative value in off-central region and negative electric field next diffuses into central region. Autonomous formation of CH plasma is seen in cycle of (f)→(a)→(b)→(c)→(d)→(e)→(f).

4. ITB Structure

The ITB structure is investigated by varying parameters: B_t / I_p =3.7T/1.3MA, 3.7T/1.7MA, 3.7T/2MA, 4.4T/2.5MA, P_{NB}=7-25 MW and $<n_e>$=2-5×10^{19} m^{-3}. The ITB width, Δ_{ITB}, and the position of ITB centre, ρ_{ITB}, are defined as the same way as in Ref.[16]: $\Delta_{ITB} = \rho_f - \rho_{sh}$ for the box-type ITB[17] where $\rho_f \sim \rho_{qmin}$ and T_i profile becomes flat for $\rho < \rho_{sh}$. In the region of Δ_{ITB}, transport is decreased to the neoclassical-level. Figure 4 (a) shows a relation between Δ_{ITB} and the ion poloidal gyroradius at the ITB centre, $\rho_{pi,ITB}$. Open circles in Fig.4(a) represent experimental data points from JT-60U[16]. The strong ITB width was proportional to $\rho_{pi,ITB}$. Simulation results represented by closed symbols in Fig.4(a) agree well with the experiments. Figures 4(b) and 4(c) shows the individual dependence of Δ_{ITB} on the poloidal magnetic field at the ITB centre, $B_{p,ITB}$, and the ion temperature at the ITB centre, $T_{i,ITB}$, respectively. In Fig.4(b), Δ_{ITB} is inverse proportional to $B_{p,ITB}$ for $T_{i,ITB}$ fixed at ~5 keV, ~8 keV and ~10 keV. Furthermore, Δ_{ITB} is proportional to the square root of $T_{i,ITB}$ for $B_{p,ITB}$ fixed at ~0.24 T in Fig.4(c). Therefore, Δ_{ITB} is clearly proportional to $\rho_{pi,ITB}$: $\Delta_{ITB} \approx 1.5\rho_{pi,ITB}$.

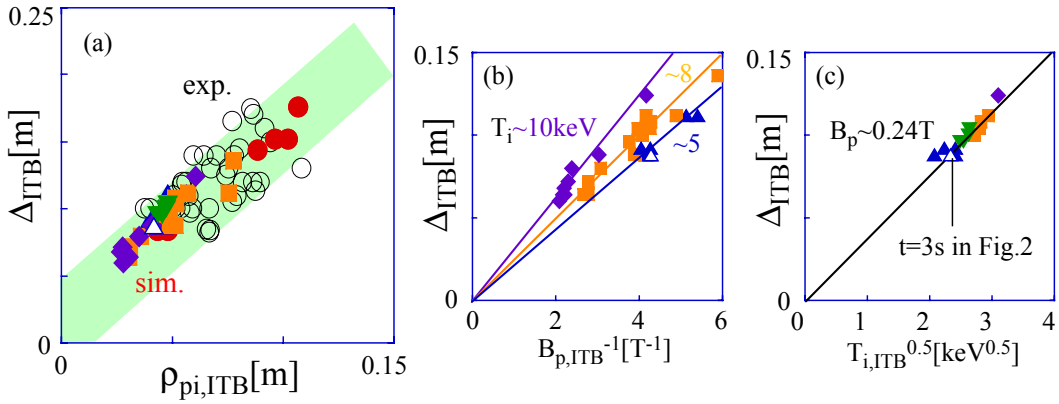

Fig.4 (a) Δ_{ITB} versus $\rho_{pi,ITB}$. (open circles: JT-60U data, closed symbols and a open triangle: simulation results) (b) Δ_{ITB} versus $B_{p,ITB}^{-1}$ for T_i^{ITB}~5 keV(triangles), 8 keV(squares) and 10 keV(diamonds). (c) Δ_{ITB} versus square root of $T_{i,ITB}$ for $B_{p,ITB}$~0.24 T. An open triangle denotes a result at t=3 s in Fig.2.

5. Autonomous Limitation of Energy Confinement

The energy confinement of the core plasma is investigated by using the same simulation results as in the previous section. The stored energy inside the ITB foot, W_{core}, is defined by $W_{core}=W_s-W_b$, where W_s and W_b denote the total stored energy in the plasma and the stored energy of the base part (assumed pressure $p_b(\rho)=p(\rho_f)$ for $\rho<\rho_f$), respectively. Figure 5(a) shows the comparison of W_{core} with the JT-60U scaling[18], $W_{scale} = 0.155\ \varepsilon_f^{-1}\ B_{p,f}^{2}\ V_{core}$, where ε_f is the inverse aspect ratio at the ITB foot, $B_{p,f}$ is the poloidal magnetic field at the outer midplane ITB foot, and V_{core} is the core volume inside the ITB foot. This scaling is equivalent to the condition of $\varepsilon_f\beta_{p,core} \approx 0.25$,

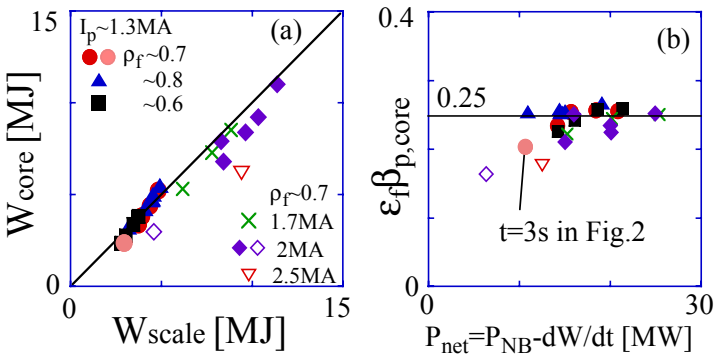

Fig.5 (a) Comparison of W_{core} with W_{scale}. (b) $\varepsilon_f\beta_{p,core}$ versus P_{net}. A shaded circle denote a result at t=3 s in Fig.2.

where the core poloidal beta is defined as $\beta_{p,core} = 4\ \mu_0 W_{core} / (3\ V_{core} B_{p,f}^2)$. As shown in Fig.5(a), values of W_{core} obtained in the simulation agree well with W_{scale}, except for two open symbols which represent data points with the insufficient heating power. Figure 5(b) shows values of $\varepsilon_f\beta_{p,core}$ as a function of the net heating power, P_{net}, defined by $P_{net}=P_{NB}-dW_s/dt$. The value of $\varepsilon_f\beta_{p,core}$ is limited for high P_{net} and the limited value is about 0.25, which is the same value derived from the scaling. For the insufficient heating power of P_{net}<10-13 MW, the value of $\varepsilon_f\beta_{p,core}$ does not reach to 0.25 as shown by two open symbols in Fig.5(b). The range of bootstrap current fraction produced by ITB, $f_{BS,ITB}$, is 0.5-0.95 for data with closed symbols in Fig.5. Even if $f_{BS,ITB}$ is reduced artificially, the limited value of 0.25 does not change. The value of $\varepsilon_f\beta_{p,core}$ defined by using the averaged $B_{p,f}$ on a magnetic surface, $<B_{p,f}>$, has a range of $\varepsilon_f\beta_{p,core}$=0.3-0.5. The upper value of $\varepsilon_f\beta_{p,core}$ defined by $<B_{p,f}>$ is limited by the condition of $f_{BS,ITB}$<1. As a result, the energy confinement inside the ITB agrees well with the energy confinement scaling based on the JT-60U data. The scaling means the autonomous limitation of stored energy in the CH plasma.

From Figs. 4 and 5, both the ITB width and the energy confinement inside ITB agree well with those in JT-60U experiments. This agreement is obtained only by using the transport model with k~0 in Eq.(1). The transport model used in the present study is validated.

6. Sustainment and Control of Autonomous CH plasmas by External Current Drive

Sustainment of CH plasmas is investigated for parameters as follows: B_t=3.7 T, I_p=1.3 MA and $<n_e>=2\text{-}3\times10^{19}$ m^{-3}. Figure 6(a) shows the time evolution of the CH radius, ρ_{CH}, and the ITB foot radius, ρ_f, for four cases: (A) P_{NB}=12 MW without the external current drive(CD), (B) P_{NB}=18 MW without CD, an exceptional case (C) employs a transport model with k=1 where the ITB expands outward and becomes like the edge transport barrier, and (D) P_{NB}=12 MW with CD. During the CH formation phase (0s<t<2s), both radii of ρ_{CH} and ρ_f can be enlarged by increasing the heating power. After the formation phase, the penetration of inductive current causes the shrinkage of the CH. The CH plasma with small ρ_{CH} and f_{BS}<1 can not be sustained as shown by the line A. The enlargement of ρ_f is the key to enhance the bootstrap current fraction, f_{BS}, which is consistent with JT-60U experiments[19]. Larger ρ_f is obtained for larger ρ_{CH}. In order to sustain the CH plasma, large ρ_{CH} with f_{BS}~1 is required. In a strongly-heated plasma, the sustainment with the full current drive by bootstrap current is achieved in the case B. Profiles of the case B are kept longer than the resistive-skin time scale. The relation of $\rho_f \sim \rho_{qmin}$ is also important for the sustainment of CH plasma. On the other hand, if $\rho_f > \rho_{qmin}$ for the transport model with k~1 in Eq.(1), the ITB radius expands continuously as shown in the case C. For the case of f_{BS}<1 (case A), we can sustain the CH configuration by adding an external CD as shown by the line D. Figure 6(b) shows the sustained profiles of j, the externally driven current density, j_{CD}, the total pressure, p, and q for the case D. To sustain this

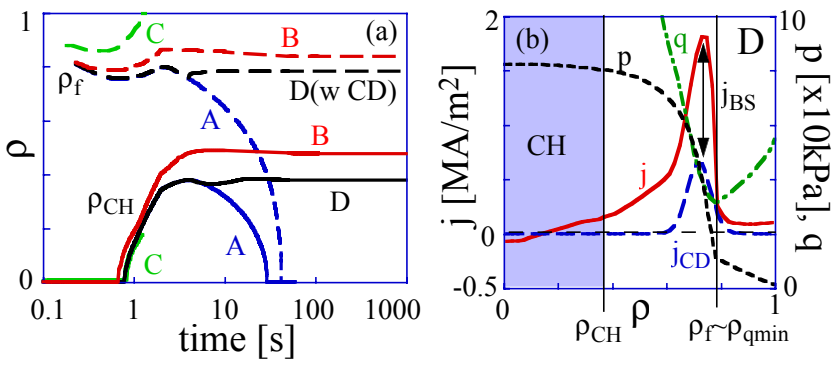

Fig.6 (a) Time evolution of ρ_{CH} and ρ_f. A: shrinkage, B: sustainment by bootstrap current, C: ρ_f expansion under condition of $\rho_f>\rho_{qmin}$. D: sustainment by external CD from t=4 s for case A. (b) Profiles of j, j_{CD}, p, and q in a sustained plasma of case D.

configuration stationarily, the externally driven current with its current fraction of $f_{CD}\approx 1-f_{BS}$ is added at the current peak as shown in Fig.6(b).

The controllability of CH plasmas by the external CD is next investigated. Figure 7(a) shows the time evolution of ρ_{CH} and ρ_f, where the CD with $f_{CD}\approx 1-f_{BS}$ starts from t=4 s for the case A as described above, externally driven current is added outside the current peak at t=4 s in the case E and inside the current peak in the case F. As shown by the line E in Fig.7(a), ρ_{CH} and ρ_f can be expanded. The process of the expansion is seen in the time evolution of j profile in Fig.7(b). While the current density gradually decreases around a position of the initial current peak, the current density increases around a position of the externally driven current. On the other hand, ρ_{CH} and ρ_f can be shrinked as shown in the line F in Fig.7(a). The shrinkage process is seen in Fig.7(c). The current peak position moves inward and reaches the CD position. Thus, the CH size and the ITB position can be controlled by the appropriate external CD.

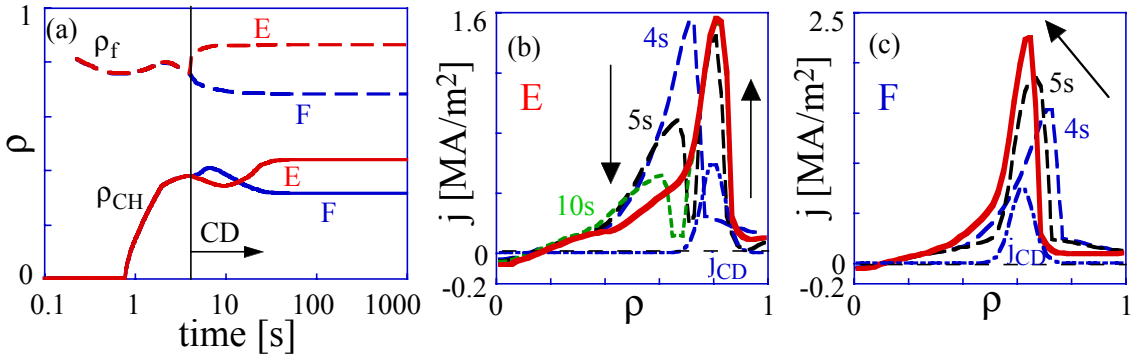

Fig.7 Controllability of CH plasma by external CD. (a) Time evolution of ρ_{CH} and ρ_f. E: j_{CD} is added outside current peak at t=4 s. F: j_{CD} is added inside current peak at t=4 s. Time evolution of j profile for (b) case E and (c) case F, where broad lines represent final profiles.

The autonomous property of CH plasmas is seen in the response to the external CD. Figure 8(a) shows the time evolution of ρ_{CH} and ρ_f where the amount of the externally driven current in the case G is larger than that in the case D as described above. In the case D, the amount of externally driven current is determined to compensate the lack of the bootstrap current fraction, i.e., $f_{CD}\approx 1-f_{BS}$. On the other hand, in the case G, the plasma just after the CD start is under the overdrive condition of $f_{BS}>1-f_{CD}$. While the ITB foot radius is kept constant, the CH radius is enlarged by the CD as shown in Fig.8(a). Therefore, the safety factor increases and the neoclassical transport is enhanced in the RS region. This results in the reduction of the energy confinement and the bootstrap current fraction. The increase of safety factor and the reduction of energy confinement are easily seen by comparing sustained profiles of the

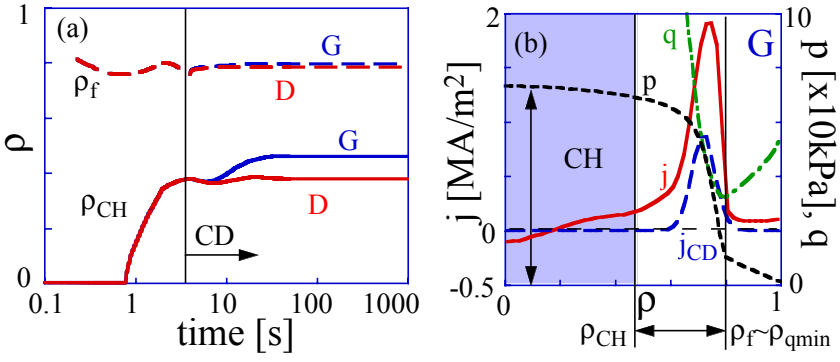

Fig.8 Autonomous response of CH plasma to external CD. (a) Time evolution of ρ_{CH} and ρ_f where case D in Fig.6 is shown again for comparison. G: External driven current is larger than that in case D. (b) Sustained profiles in case G. Safety factor is more increased in RS region and energy confinement (p at centre) is lower compared with those in case D as shown in Fig.6(b).

case G in Fig.8(b) with those of the case D in Fig.6(b). As a result, the relation of $f_{BS} \approx 1 - f_{CD}$ is recovered and the CH plasma is sustained. The CH plasma is found to respond autonomically to the external CD.

7. Conclusions

Profile formation and sustainment of tokamak plasmas with the CH have been investigated by using 1.5D transport simulations with a model of the current limit inside the CH on the basis of the ATMI equilibrium. We found that a transport model with the sharp reduction of anomalous transport in the RS region can reproduce the time evolution of profiles observed in JT-60U experiments. The transport becomes neoclassical-level in the RS region, which results in the formation of profiles with ITB and CH. The CH plasma has an autonomous property because of the strong interaction between a pressure profile and a current profile through the large bootstrap current fraction. The ITB width determined by the neoclassical-level transport agrees well with that measured in JT-60U. The energy confinement inside the ITB agrees well with the JT-60U scaling. This scaling means the autonomous limitation of energy confinement in the CH plasma. The plasma with the large CH is sustained with the full current drive by the bootstrap current. The plasma with the small CH and the small bootstrap current fraction shrinks due to the penetration of inductive current. This shrink is prevented by adding the external CD at the current peak and making the full current drive condition. The CH size can be expanded by adding the external CD outside the current peak, or can be reduced by adding inside the current peak. The CH plasma is found to respond autonomically to the external CD.

Acknowledgements: We would like to thank Drs. T. Fujita and Y. Sakamoto for fruitful discussion and comments. This work was partly supported by JSPS, Grant-in-Aid for Scientific Research.

References

[1] FUJITA, T., et al., Phys. Rev. Lett., **87** (2001) 245001.
[2] HAWKES, N.C., et al., Phys. Rev. Lett., **87** (2001) 115001.
[3] TAKIZUKA, T., J. Plasma Fusion Res., **78** (2002) 1282.
[4] HUYSMANS, G.T.A., et al., Phys. Rev. Lett., **87** (2001) 245002.
[5] BRESLAU, J.A., et al., Phys. Plasma, **10** (2003) 1665.
[6] ISHIZAWA, A., et al., Phys. Plasma, **10** (2003) 3017.
[7] MARTINOV, A.A., et al., Phys. Rev. Lett., **91** (2003) 085004.
[8] HAWKES, N.C., et al., Plasma Phys. Control. Fusion, **44** (2002) 1105.
[9] TALA, T.J.J., et al., Plasma Phys. Control. Fusion, **44** (2002) 1181.
[10] HAYASHI, N., et al., J. Plasma Fusion Res., **80** (2004) 605.
[11] KIKUCHI, M., et al., Nucl. Fusion, **30** (1990) 343.
[12] TAKENAGA, H., et al., Nucl. Fusion, **43** (2003) 1235.
[13] FUKUYAMA, A., et al., Plasma Phys. Control. Fusion, **37** (1995) 611.
[14] WALTZ, R.E., et al. Phys. Plasmas, **4** (1997) 2482.
[15] FUJITA, T., et al., et al., Nucl. Fusion, **38** (1998) 207.
[16] SAKAMOTO, Y., et al., Nucl. Fusion, **41** (2001) 865.
[17] SHIRAI, H., et al., Nucl. Fusion, **39** (1999) 1713.
[18] TAKIZUKA, T., et al., Plasma Phys. Control. Fusion, **44** (2002) A423.
[19] FUJITA, T., et al., Nucl Fusion, **42** (2002) 1800.